Eur. Phys. J. D **44**, 23–33 (2007)
DOI: 10.1140/epjd/e2007-00161-2

THE EUROPEAN
PHYSICAL JOURNAL D

Lifetime and transition probability determination in xenon ions

The cases of Xe VII and Xe VIII

É. Biémont[1,2,a], M. Clar[1], V. Fivet[2], H.-P. Garnir[1], P. Palmeri[2], P. Quinet[1,2], and D. Rostohar[1]

[1] Institut de Physique Nucléaire, Atomique et de Spectroscopie, Université de Liège, Sart Tilman (Bât. B15), 4000 Liège, Belgium
[2] Astrophysique et Spectroscopie, Université de Mons-Hainaut, 7000 Mons, Belgium

Received 3rd January 2007 / Received in final form 8th February 2007

Abstract. Radiative lifetimes have been calculated for 15 levels of Xe VII belonging to the configurations $5s5p$, $5p^2$, $5s5d$, $5s6s$, $5p5d$, $4f5p$, $5p5d$ and $5s5f$ and for 4 levels of the $5p$ and $5d$ configurations of Xe VIII. A relativistic Hartree-Fock approach including core-polarization effects, on the one hand, and a purely relativistic multiconfiguration Dirac-Fock method, on the other hand, have been used for the calculations. The accuracy of the present set of results has been assessed through comparisons with radiative lifetime measurements obtained by beam-foil spectroscopy. A good agreement between theory and experiment is observed for most of the levels. A new set of transition probabilities is proposed for 169 transitions of Xe VII and 45 transitions of Xe VIII.

PACS. 34.50.Fa Electronic excitation and ionization of atoms – 32.30.Jc Visible and ultraviolet spectra

1 Introduction

The spectra of Xe^{6+} (Xe VII) and Xe^{7+} (Xe VIII) are still poorly known not only regarding term analysis but also concerning line intensity and radiative transition probability determination. Such data however are strongly needed in different fields of physics including astrophysics and plasma physics.

In astrophysics for example, the detection of collisionally excited lines of krypton and xenon ions in the spectrum of the planetary nebula NGC 7027 has been reported by Péquignot and Baluteau [1] and has stimulated later on calculations of collision strengths for electron impact excitation in xenon ions by Schöning and Butler [2].

In plasma physics, spectroscopic and radiative data are needed for the investigation of excitation mechanisms and characterization of multi-ionic xenon lasers [3].

In addition, performing calculations of atomic structures in heavy multicharged ions like xenon ions is attractive for the theoreticians because relativity and correlation effects must be considered simultaneously in the calculations which is a difficult challenge.

In view of this fragmentary knowledge of the transition probabilities and lifetimes in Xe VII and Xe VIII, we report in the present work on a detailed theoretical analysis of the radiative parameters of these ions for transitions or levels not considered previously. Two different theoretical approaches i.e. a relativistic Hartree-Fock (HFR) method with core-polarization (CP) effects included and a fully relativistic multiconfiguration Dirac-Fock (MCDF) methodology have been retained for providing the required data. The theoretical results have been compared with radiative lifetimes obtained using the beam-foil (BF) spectroscopy technique, one of the rare methods able to provide experimental data in these multicharged ions. An overall good agreement between theory and experiment has been observed allowing to assess the reliability of the new data.

The present paper is an extension of the work recently carried out in Xe V [4] and Xe VI ions [5].

2 Previous work

2.1 Xe VII

Xe VII belongs to the cadmium isoelectronic sequence. The experimental lifetimes and transition probabilities in this ion are still fragmentary.

An early report on Xe VII and Xe VIII line identification in atomic spectra was published by Fawcett et al. [6] who used a zeta pinch device for producing a plasma and analyzed the wavelength region 40–100 nm. More recent work on this ion has been reported and was based on beam-foil spectroscopy [7–10] and on the analysis of spark spectra [11].

The photon emission, from 60-keV Xe^{6+} ions colliding with Na and Ar, was recorded by Wang et al. [12]

[a] e-mail: E.Biemont@ulg.ac.be

in the 35–800-nm wavelength range. Twenty-two new Xe VII lines were classified and nine new energy levels were established.

The ground state of Xe^{6+} is $4d^{10}5s^2\ ^1S_0$. The excited levels belong to the configurations $5snp$ ($n = 5$–7), $5p^2$, $4f5s$, $5snd$ ($n = 5$–6), $4f5p$, $5p5d$, $5s5f$, $5p6s$, $5sns$ ($n = 6$–7) and $4d^95s^2nl$ ($nl = 4f, 5f, 6p$). An extensive investigation of the Xe VII level scheme is due to Churilov and Joshi [13] who extended or complemented previous work [6–9, 11, 14–17].

72 levels of Xe VII are quoted in the NIST compilations [18, 19].

The cadmium isoelectronic sequence (including Xe VII) has attracted the interest of a number of theoreticians who compared different calculational approaches. Most of these efforts, however, were concentrated on the resonance transitions. Indeed, the $5s^2\ ^1S_0$–$5s5p\ ^{1,3}P^\circ_1$ transitions were studied by a number of authors [20–25, 27–29]. These resonance and intercombination transitions have also been reconsidered by Biémont et al. [26] for $48 \leq Z \leq 57$ using the HFR approach, including a CP potential, and the MCDF method, taking the valence and the core-valence correlation effects into account. As pointed out in this work, the discrepancies observed between theory and experiment for the singlet-singlet transition indicate that some experimental data are in need of revision along the sequence.

2.2 Xe VIII

Experimental work in Xe^{7+} ion is also rather sparse [10, 30–32].

A number of theoretical investigations were focused on the silver isoelectronic sequence (including Xe VIII) [33–36]. More specifically, the $5s\ ^2S_{1/2}$–$5p\ ^2P^\circ_{1/2,3/2}$ resonance transitions have attracted the interest of a number of theoreticians [37–39].

The ground state of Xe VIII is $4d^{10}5s\ ^2S_{1/2}$ and one-electron configurations are known experimentally up to $9s$, $9p$, $9d$, $9f$, $9g$, $9h$, 9l, $10i$ and $10k$, respectively [18, 19]. Some levels of the doubly excited configurations $4d^95s5p$ and $4d^95s4f$ have also been determined experimentally.

Early line identifications in the spectrum of Xe VIII are due to Fawcett et al. [6]. The Xe VIII spectrum has been investigated by the use of different types of sources including BF spectroscopy [7, 40], electric sparks [41, 42] and discharge tubes [43]. The resonance lines of Ag-like xenon have been reported in different publications [15, 41, 42]. An analysis of some highly excited levels of Xe VIII and Xe IX ions has been published by Churilov and Joshi [44]. Additional work has appeared in different papers [31, 32].

82 levels of Xe VIII are quoted in the NIST compilations [18, 19] while the most recent compilation of wavelengths and energy levels of xenon ions is due to Saloman [19] who adopted for Xe VII and Xe VIII the level values from references [12, 13, 15, 45] and references [16, 31, 41, 44], respectively.

3 Pseudo-relativistic Hartree-Fock calculations

Calculations of energy levels and transition probabilities in Xe VII and Xe VIII have been carried out using the HFR approach implemented in the Cowan's suite of computer codes [46] modified for taking CP effects into account. Although based on the Schrödinger equation, the HFR method incorporates the most important relativistic effects, i.e. the mass and velocity contributions and the Darwin correction. CI can be considered in the calculations in a very flexible way. Furthermore, the CP effects have been included through the use of a pseudo-potential and a correction to the dipole operator leading to the HFR + CP approach (for a detailed description, see e.g. [47, 48]). This method has been combined with a least-squares optimization process of the radial parameters in order to minimize the discrepancies between Hamiltonian eigenvalues and experimental energy levels when available.

3.1 Xe VII

For Xe VII, we focused our calculations on the lifetimes of levels belonging to the configurations $4d^{10}5s5p$, $4d^{10}5p^2$, $4d^{10}5s5d$, $4d^{10}5s6s$, $4d^{10}4f5p$, $4d^{10}5p6d$ and $4d^{10}5s5f$. The configurations explicitly retained in the CI expansion were of the type $4d^{10}nln'l'$ with $nl = 4f$, $5s$, $5p$, $5d$ and $n'l' = 4f$, $5s$, $5p$, $5d$, $5f$, $5g$, $6s$, $6p$, $6d$, $6f$, $6g$ and $6h$.

The correlations between the 2 valence electrons and the core subshells $1s^22s^22p^63s^23p^63d^{10}4s^24p^64d^{10}$ were considered within the framework of a CP potential and a correction to the dipole transition operator [47]. The estimate of these contributions requires the knowledge of the dipole polarisability of the ionic core, α_d and of the cut-off radius r_c. For the first parameter, we used the value computed by Fraga et al. [49] for the Xe^{8+} ion, i.e. $\alpha_d = 0.88\ a_0^3$, while the cut-off radius, r_c, was chosen equal to 0.86 a_0 which corresponds to the HFR value $\langle r \rangle$ of the outermost core orbital $4d^{10}$.

The semi-empirical optimization of the radial integrals was applied to all the experimentally known configurations of the CI expansion, i.e. $4d^{10}5s^2$, $4d^{10}5s5p$, $4d^{10}5p^2$, $4d^{10}4f5s$, $4d^{10}5s5d$, $4d^{10}5s6s$, $4d^{10}4f5p$, $4d^{10}5p5d$, $4d^{10}5s6p$, $4d^{10}5s5f$, $4d^{10}5p6s$ and $4d^{10}5s6d$, using the energy level values compiled in the NIST Atomic Spectra Database [18]. The Slater parameters, not adjusted in this semi-empirical approach, were scaled down by 0.90 according to a procedure outlined in reference [46]. The spin-orbit parameters were left at their ab initio values. The introduction of a scaling factor is justified on theoretical grounds [46] and the choice of the numerical value (i.e. 0.90) is suited for highly charged ions [46]. It was verified that altering the present scaling factors by ±5% does not change significantly the radiative parameters.

In the even parity, 27 levels were fitted with 17 parameters giving rise to a standard deviation of 377 cm^{-1}. Concerning the odd parity, 32 levels were fitted with 20 parameters resulting in a standard deviation somewhat smaller (250 cm^{-1}).

Table 1. Adopted radial parameters values in the HFR + CP calculations for Xe VII. All the values are given in cm^{-1}.

Configuration	Parameter	Adopted value	σ^a
$5s^2$	E_{av}	6729	386
$5s6s$	E_{av}	358 541	301
	$G^0(5s, 6s)$	4072	270
$5s5d$	E_{av}	293 262	221
	ζ_{5d}	1067	212
	$G^2(5s, 5d)$	23 724	1526
$5s6d$	E_{av}	478 427	224
	ζ_{6d}	384	fixed
	$G^2(5s, 6d)$	8237	fixed
$5p^2$	E_{av}	249 085	240
	$F^2(5p, 5p)$	48 330	1354
	α	1161	173
	ζ_{5p}	11 556	207
$4f5p$	E_{av}	398 881	113
	ζ_{4f}	206	81
	ζ_{5p}	11 558	213
	$F^2(4f, 5p)$	42 826	1366
	$G^2(4f, 5p)$	31 093	987
	$G^4(4f, 5p)$	20 697	1416
$5s5p$	E_{av}	118 690	137
	ζ_{5p}	11 702	219
	$G^1(5s, 5p)$	59482	515
$5s6p$	E_{av}	407 717	171
	ζ_{6p}	4682	231
	$G^1(5s, 6p)$	5684	802
$5s4f$	E_{av}	275 867	128
	ζ_{4f}	184	100
	$G^3(5s, 4f)$	32 029	1043
$5s5f$	E_{av}	463 458	134
	ζ_{5f}	89	fixed
	$G^3(5s,5f)$	5096	1179
$5p6s$	E_{av}	481 478	137
	ζ_{5p}	11 183	196
	$G^1(5p, 6s)$	6701	660
$5p5d$	E_{av}	418 796	84
	ζ_{5p}	11 366	213
	ζ_{5d}	1145	134
	$F^2(5p, 5d)$	40 381	932
	$G^1(5p, 5d)$	45 053	439
	$G^3(5p, 5d)$	27 933	932

[a]Standard deviation.

The energy parameter values (in cm^{-1}) are reported in Table 1 which contains only the parameters varied during the calculations. A comparison between experimental and calculated energy level values is shown in Table 2 where we report also the calculated percentage compositions in LS coupling (only the three main components of the eigenvectors are given in the table).

3.2 Xe VIII

In the Xe^{7+} ion, the lifetimes of the levels of the first excited levels, i.e. $5p\ ^2P^\circ_{1/2,3/2}$, and of the $5d\ ^2D_{3/2,5/2}$ states have been investigated. The CI expansion included the following configurations: $5s$, $6s$, $5p$, $6p$, $5d$, $6d$, $4f$, $5f$, $6f$, $5g$, $6g$ and $6h$.

As in Xe VII, the correlations between the valence electron and the core electrons were taken into account through a polarization potential and a correction to the dipole transition operator [47]. We have considered the same core as for the Xe VII calculations, i.e. $1s^22s^22p^63s^2$–$3p^63d^{10}4s^24p^64d^{10}$ Xe IX ionic core and, consequently, we have adopted the same value for the dipole polarizability and the cut-off radius.

A least-squares fit has been carried out in order to minimize the discrepancies between the eigenvalues of the Hamiltonian and the energy level values recently reported by Gallardo et al. [32]. 22 radial integrals (the average energies and the spin-orbit parameters) have been adjusted to fit the 22 energy levels generated from the abovementioned CI expansion. The characteristics of the fit are therefore trivial. Table 3 shows the numerical values of the parameters obtained in this semi-empirical process.

In order to check the reliability of our HFR+CP model, an extended HFR model retaining explicitly in the multiconfiguration expansion the $4d^{10}nl$ Rydberg series up to $n = 10$ and all the configurations with an open $4d$ subshell was tested. This latter model, in which the $4d^{10}ns$ (n = 5–10), $4d^{10}nd$ (n = 5–10), $4d^{10}ng$ (n = 5–10), $4d^{10}ni$ (n = 7–10), $4d^95s^2$, $4d^95s5d$, $4d^95p^2$, $4d^95p5f$, $4d^95d^2$, $4d^94f^2$, $4d^95f^2$, $4d^94f5p$, $4d^94f5f$ (even parity) and $4d^{10}np$ (n = 5–10), $4d^{10}nf$ (n = 4–10), $4d^{10}nh$ (n = 6–10), $4d^{10}nk$ (n = 8–10), $4d^95s5p$, $4d^95s5f$, $4d^95d5f$, $4d^94f5s$, $4d^94f5d$, $4d^95p5d$ (odd parity) configurations were included, gave rise to computed radiative lifetimes for the $5p$ and $5d$ states in excellent agreement (in fact within a few %) with the ones obtained with our HFR+CP model.

The HFR + CP lifetime values are reported in Table 4 (Col. 5).

4 Relativistic Dirac-Fock calculations

The Z-values and ionization stages considered in the present work should be sufficiently low for the HFR approximation to be adequate for the treatment of relativistic effects. To verify this point, we have also performed fully relativistic MCDF calculations using the latest version of GRASP, the General-purpose Relativistic Atomic Structure Package developed by Norrington [50] from the original code of Grant and co-workers [51–53]. The computations were performed with the extended average level (EAL) option, optimizing a weighted trace of the Hamiltonian using level weights proportional to $2J + 1$.

In Xe VII, the following non-relativistic configurations were included in the model: $4d^{10}5s^2$, $4d^{10}5p^2$, $4d^{10}5d^2$, $4d^{10}4f^2$, $4d^{10}5s5d$, $4d^{10}5s6s$, $4d^{10}5s6d$, $4d^{10}4f5p$, $4d^95s5p^2$, $4d^95s^25d$, $4d^95s^26s$ (even parity) and $4d^{10}5s5p$, $4d^{10}5s6p$, $4d^{10}4f5s$, $4d^{10}5s5f$, $4d^{10}5p5d$, $4d^{10}4f5d$, $4d^{10}5p6s$, $4d^95s^25p$, $4d^94f5s^2$ and $4d^95s^25f$ (odd parity).

In Xe VIII, the MCDF approach was used with the non-relativistic configurations $4d^{10}5s$, $4d^{10}5d$, $4d^{10}6s$, $4d^{10}6d$, $4d^95s^2$, $4d^95p^2$, $4d^95s5d$, $4d^95d^2$ (even parity)

Table 2. Experimental and calculated energy level (in cm^{-1}) in Xe VII. Only the largest (≥1) percentage compositions are given.

$E_{exp}{}^a$	$E_{calc}{}^b$	ΔE^c	J	LS-coupling composition^d (%)
0	0	0	0	98 $5s^2$ ^{1}S +2 $5p^2$ ^{1}S
96 141	96 194	−53	0	100 $5s5p$ ^{3}P°
100 451	100 386	65	1	96 $5s5p$ ^{3}P° + 4 $5s5p$ ^{1}P°
113 676	113 685	−9	2	100 $5s5p$ ^{3}P°
143 259	143 257	2	1	94 $5s5p$ ^{1}P° + 4 $5s5p$ ^{3}P° + 2 $5p5d$ ^{1}P°
223 673	223 435	238	0	88 $5p^2$ ^3P + 11 $5p^2$ ^{1}S
234 685	235 022	−337	1	100 $5p^2$ ^3P
236 100	236 209	−109	2	55 $5p^2$ ^{1}D + 34 $5p^2$ ^3P + 11 $5s5d$ ^{1}D
251 853	251 598	255	2	65 $5p^2$ ^3P + 25 $5p^2$ ^{1}D + 9 $5s5d$ ^{1}D
272 581	272 565	16	2	100 $5s4f$ ^{3}F°
272 812	272 839	−27	3	100 $5s4f$ ^{3}F°
273 245	273 235	10	4	100 $5s4f$ ^{3}F°
273 208	273 239	−31	0	85 $5p^2$ ^{1}S + 12 $5p^2$ ^3P + 2 $5s^2$ ^{1}S
279 282	279 288	−6	3	98 $5s4f$ ^{1}F° + 1 $5p5d$ ^{1}F°
287 772	287 766	6	1	99$5s5d$ ^{3}D + 1 $5p4f$ ^{3}D
288 712	288 721	−9	2	99$5s5d$ ^{3}D + 1 $5p4f$ ^{3}D
290 340	290 334	6	3	99 $5s5d$ ^{3}D + 1 $5p4f$ ^{3}D
307 542	307 538	4	2	76 $5s5d$ ^{1}D + 1 8$5p^2$ ^{1}D + 5 $5p4f$ ^{1}D
354 833	354 833	0	1	99 $5s6s$ ^{3}S + 1 $5p6p$ ^{3}S
361 671	361 671	0	0	98 $5s6s$ ^{1}S + 2 $5p6p$ ^{1}S
382 356	382 086	270	3	61 $5p4f$ ^{3}G + 33 $5p4f$ ^{1}F + 5 $5p4f$ ^{3}F
385 422	385 592	−170	3	47 $5p4f$ ^{3}F + 24 $5p4f$ ^{3}D + 24 $5p4f$ ^{1}F
386 172	386 057	115	4	50 $5p4f$ ^{3}G + 38 $5p4f$ ^{3}F + 11 $5p4f$ ^{1}G
386 811	387 062	−251	2	81 $5p4f$ ^{3}F + 11 $5p4f$ ^{3}D + 7 $5p4f$ ^{1}D
393 792	393 619	173	2	81 $5p5d$ ^{3}F° + 16 $5p5d$ ^{1}D° + 1 $5p5d$ ^{3}D°
398 027	398 210	−183	3	35 $5p4f$ ^{1}F + 33 $5p4f$ ^{3}G + 31 $5p4f$ ^{3}F
399 987	399 916	71	4	57 $5p4f$ ^{3}F + 43 $5p4f$ ^{3}G
400 666	400 534	132	0	97 $5s6p$ ^{3}P° + 2 $5p5d$ ^{3}P° + 1 $5p6s$ ^{3}P°
400 893	401 025	−132	1	74 $5s6p$ ^{3}P° + 23 $5s6p$ ^{1}P° + 2 $5p5d$ ^{3}P°
401 595	401 313	282	5	100 $5p4f$ ^{3}G
401 413	401 362	51	3	89 $5p5d$ ^{3}F° + 6 $5p5d$ ^{3}D° + 3 $5p5d$ ^{1}F°
404 548	404 709	−161	2	33 $5p5d$ ^{1}D° + 26 $5p5d$ ^{3}P° + 22 $5s6p$ ^{3}P°
404 979	405 059	−80	3	73 $5p4f$ ^{3}D + 18 $5p4f$ ^{3}F + 8 $5p4f$ ^{1}F
406 342	406 488	−146	2	78 $5p4f$ ^{3}D + 16 $5p4f$ ^{3}F + 5 $5p4f$ ^{1}D
407 802	407 837	−35	1	67 $5s6p$ ^{1}P° + 18 $5s6p$ ^{3}P° + 6 $5p5d$ ^{3}D°
408 347	408 338	9	2	73 $5s6p$ ^{3}P° + 19 $5p5d$ ^{1}D° + 3 $5p5d$ ^{3}D°
408 767	408 856	−89	1	99 $5p4f$ ^{3}D + 1 $5s5d$ ^{3}D
411 551	410 879	672	4	87 $5p4f$ ^{1}G + 7 $5p4f$ ^{3}G + 4 $5p4f$ ^{3}F
411 022	411 148	−126	1	65 $5p5d$ ^{3}D° + 15 $5p5d$ ^{3}P° + 7 $5p5d$ ^{1}P°
412 567	412 372	195	4	97 $5p5d$ ^{3}F° + 2 $5s5f$ ^{3}F°
416 357	416 872	−515	2	81 $5p4f$ ^{1}D + 10 $5p4f$ ^{3}D + 3 $5p4f$ ^{3}F
417 240	417 349	−109	2	43 $5p5d$ ^{3}D° + 28 $5p5d$ ^{1}D° + 19 $5p5d$ ^{3}P°
423 028	423 132	−104	3	86 $5p5d$ ^{3}D° + 8 $5p5d$ ^{3}F° + 5 $5p5d$ ^{1}F°
424 188	424 305	−117	0	97 $5p5d$ ^{3}P° + 2 $5s6p$ ^{3}P° + 1 $4f5d$ ^{3}P°
424 567	424 537	30	1	74 $5p5d$ ^{3}P° + 23 $5p5d$ ^{3}D° + 2 $5s6p$ ^{3}P°
425 234	425 320	−86	2	53 $5p5d$ ^{3}P° + 41 $5p5d$ ^{3}D° + 4 $5p5d$ ^{1}D°
438 428	437 792	636	3	74 $5p5d$ ^{1}F° + 15 $5s5f$ ^{1}F° + 7 $5p5d$ ^{3}D°
441 376	441 708	−332	1	85 $5p5d$ ^{1}P° + 6 $5p5d$ ^{3}D° + 4 $5p5d$ ^{3}P°
462 702	462 630	72	2	98 $5s5f$ ^{3}F° + 1 $5p5d$ ^{3}F°
462 791	462 858	−67	3	98 $5s5f$ ^{3}F° + 2 $5p5d$ ^{3}F°
463 159	463 171	−12	4	97 $5s5f$ ^{3}F° + 2 $5p5d$ ^{3}F°
467 700	467 814	−114	3	84 $5s5f$ ^{1}F° + 14 $5p5d$ ^{1}F° + 1 $5p5g$ ^{1}F°
468 777	468 842	−65	0	99 5p6s ^{3}P° + 1 $5s6p$ ^{3}P°
470 805	470737	68	1	79 $5p6s$ ^{3}P° + 18 $5p6s$ ^{1}P° + 1 $5s6p$ ^{1}P°
475 990	475 718	272	1	96 $5s6d$ ^{3}D + 3 $5p6p$ ^{3}D
476 220	476 248	−28	2	96 $5s6d$ ^{3}D + 2 $5p6p$ ^{3}D + 1 $5s6d$ ^{1}D
476 800	477 029	−229	3	98 $5s6d$ ^{3}D + 1 $5p6p$ ^{3}D
-	479 359	–	2	92 $5s6d$ ^{1}D + 5 $5p6p$ ^{1}D + 1 $5p4f$ ^{1}D
485 435	485 422	13	2	99 $5p6s$ ^{3}P° + 1 $5s6p$ ^{3}P°
489 957	489 971	−14	1	77 $5p6s$ ^{1}P° + 19 $5p6s$ ^{3}P° + 3 $5s6p$ ^{1}P°

[a] From NIST [18]; [b] HFR + CP (see the text); [c] $E_{exp} - E_{calc}$;
[d] the three main components (larger than 1%) are tabulated.

Table 3. Adopted radial parameter values in the HFR + CP calculations for Xe VIII. All the values are given in cm^{-1}.

Configuration	Parameter	Adopted value
$5s$	E_{av}	0
$6s$	E_{av}	395 497
$5d$	E_{av}	311 645
	ζ_{5d}	1171
$6d$	E_{av}	528 246
	ζ_{6d}	548
$5g$	E_{av}	570 268
	ζ_{5g}	0
$6g$	E_{av}	656 891
	ζ_{6g}	0
$5p$	E_{av}	128 857
	ζ_{5p}	12390
$6p$	E_{av}	448 308
	ζ_{6p}	4930
$4f$	E_{av}	265 475
	ζ_{4f}	157
$5f$	E_{av}	497 830
	ζ_{5f}	125
$6f$	E_{av}	616 562
	ζ_{6f}	97
$6h$	E_{av}	659 228
	ζ_{6h}	0

and $4d^{10}5p$, $4d^{10}6p$, $4d^{10}4f$, $4d^95s5p$, $4d^94f5s$, $4d^94f5d$, $4d^95p5d$ (odd parity). In both ions, the calculations were performed with the inclusion of the relativistic two-body Breit interaction and of the quantum electrodynamic (QED) corrections due to self-energy and vacuum polarization using the routines developed by McKenzie et al. [52]. In these routines, the leading corrections to the Coulomb repulsion between electrons in quantum electrodynamics are considered as a first-order perturbation using the transverse Breit operator given by Grant et al. [51]. The second-order vacuum polarization corrections are evaluated using the prescription of Fullerton and Rinker [54], and the self-energy contributions were estimated by interpolating the values obtained by Mohr [55,56] for $1s$, $2s$ and $2p$ Coulomb orbitals. The nuclear effects were estimated by considering a uniform charge distribution in the atomic nucleus. In both Xe VII and Xe VIII, it was verified that the average deviation of MCDF calculated energies from experimental values was less than 1%.

5 Discussion about the theoretical results

The HFR+CP and MCDF lifetime values calculated in Xe VII and Xe VIII are presented in Table 4 where they are compared with the experimental values measured in the present work.

One can observe that both sets of theoretical results (see Cols. 5 and 6 of Tab. 4) are in very good agreement if we exclude the $5p^2\ ^3P_{0,1,2}$, the $5p^2\ ^1S_0$ and the $4f5p$ $^3D_3$, $^1G_4$ levels in Xe VII. This is mainly due to the fact that core-valence correlations are more completely taken into account in the HFR+CP approach than in the MCDF model adopted for this ion including only a few configurations with one hole in the $4d$ subshell.

The method used in reference [13] is similar to ours and led to better standard deviations. A detailed comparison of the results obtained in the present work and those of [13] shows that our transition probabilities are lower by about 20% (for 82 transitions). The differences in standard deviations can be explained by the consideration of a more extended configuration-interaction expansion in our model that introduces more uncertainties in our fits due to the unknown positions of numerous configurations.

In the case of Xe VIII, oscillator strengths were published by Gallardo et al. [32] for all the transitions which they observed in their spectrum. They also used Cowan's codes including a more extended CI expansion (going up to $n = 10$ and including a few configurations with an open $4d$ shell). However, it seems obvious that their model is not sufficient to take into account all the core-valence interactions that affect some levels. More particularly, Gallardo et al. [32] obtained a $\log gf$-value of 0.172 for the transition $5s\ ^2S_{1/2}$–$5p\ ^2P^\circ_{3/2}$ (strangely they did not observe the transition $5s\ ^2S_{1/2}$–$5p\ ^2P^\circ_{1/2}$ falling in their wavelength range at ≈85.8 nm). This corresponds to a calculated lifetime for the $5p\ ^2P^\circ_{3/2}$ level of 0.22 ns which is ≈30% lower than our theoretical values (τ_{HFR+CP} = 0.31 ns and τ_{MCDF} = 0.33 ns) and our BF measurement ($\tau_{exp} = 0.35 \pm 0.02$ ns). However their result agrees with our HFR value obtained without consideration of the CP contributions, i.e. τ_{HFR} = 0.22 ns.

In Tables 5 and 6, we report the oscillator strengths and radiative transition probabilities for Xe VII and Xe VIII lines, respectively, as obtained using our HFR+CP model. This approach has been preferred to the MCDF one because, as already mentioned, the core-valence interactions were more completely taken into account in that model.

6 Measurements

In order to assess the reliability of the calculations, comparisons with experimental results have been performed. More precisely, lifetimes of Xe VII and Xe VIII levels have been measured by the BF method [57], one of the rare methods able to produce the multicharged ions investigated in the present work.

A Xe^+ beam of ≈0.15 A was produced by the 2MV Van de Graaff accelerator of Liège University equipped with a conventional radio-frequency source. The beam was analyzed by a magnet and focused inside a target chamber. Beams of energies up to 2 MeV could be produced. Inside the chamber, the beam was excited and ionized by passing through a very thin (∼20 $\mu g/cm^2$) home-made carbon foil. Just after the foil, the light, emitted by the excited ions, was observed at right angle with a Seya-Namioka-type spectrometer. The entrance slit of the spectrometer had a width of 100 μm and was situated at 10 mm from the axis of the 6 mm diameter ion beam. The grating

Table 4. Comparison between calculated and measured lifetime values (in ns) for some Xe VII and Xe VIII levels.

Ion	Configuration	Level	Energy (cm^{-1})	τ_{HFR+CP} (ns)	τ_{MCDF} (ns)	τ_{BFS} (ns)	Depopulation channel [a]
Xe VII	$4d^{10}5s5p$	$^1P^\circ_1$	143 259	0.14	0.14	0.19(1)	$5s^2\ ^1S_0$
	$4d^{10}5p^2$	$^3P_0$	223 673	0.21	0.14	0.25(3)	$5s5p\ ^3P^\circ_1$
		$^3P_1$	234 685	0.17	0.12	0.19(2)	$5s5p\ ^3P^\circ_{0,1}$
		$^3P_2$	251 853	0.21	0.13	0.23(2)	$5s5p\ ^3P^\circ_{1,2}$ [b]
	$4d^{10}5p^2$	$^1D_2$	236 100	0.41	0.37	0.36(4)	$5s5p\ ^3P^\circ_1$ [c]
	$4d^{10}5p^2$	$^1S_0$	273 208	0.151	0.107		
	$4d^{10}5s5d$	$^3D_1$	287 772	0.07	0.06	0.08(1)*	$5s5p\ ^3P^\circ_0$ [d]
		$^3D_2$	288 712	0.07	0.06	0.08(2)*	$5s5p\ ^3P^\circ_{1,2}$
		$^3D_3$	290 340	0.08	0.07	0.08(2)*	$5s5p\ ^3P^\circ_2$
	$4d^{10}5s6s$	$^3S_1$	354 833	0.04	0.05	0.06(2)	$5s5p\ ^3P^\circ_2$ [e]
	$4d^{10}4f5p$	$^3D_3$	404 979	0.27	0.22		
	$4d^{10}4f5p$	$^1G_4$	411 551	0.40	0.32		
	$4d^{10}5p5d$	$^1F^\circ_3$	438 428	0.05	0.05	0.06(1)	$5p^2\ ^1D_2$
	$4d^{10}5p5d$	$^1P^\circ_1$	441 376	0.07	0.06	0.08(2)	$5p^2\ ^1S_0$
	$4d^{10}5s5f$	$^3F^\circ_4$	463 159	0.06	0.05	0.06(1)*	$5s5d\ ^3D_3$
Xe VIII	$4d^{10}5p$	$^2P^\circ_{1/2}$	116 467	0.48	0.53	0.52(3)	$5s\ ^2S_{1/2}$
		$^2P^\circ_{3/2}$	135 052	0.31	0.33	0.35(2)	$5s\ ^2S_{1/2}$
	$4d^{10}5d$	$^2D^\circ_{3/2}$	309 888	0.07	0.06	0.10(2)	$5p\ ^2P_{1/2}$
		$^2D^\circ_{5/2}$	312 816	0.08	0.07	0.14(2)	$5p\ ^2P_{3/2}$

* Obtained through constrained fit (see the text). [a] We indicate the lower level of the depopulation transition used for the measurements; [b] the line $5s5p\ ^3P^\circ_2$–$5p^2\ ^3P_1$ is blended with a Xe IX transition; [c] the $5s5p\ ^3P^\circ_1$–$5p^2\ ^1D_2$ transition is blended with a strong Xe IX line; [d] possible blend with a strong Xe IX line at 52.1783 nm. According to the NIST Atomic database [18], the transition to $5s5p\ ^3P^\circ_1$ is weak and blended with $5p5d\ ^3D^\circ_1$–$5p^2\ ^3P_0$ in Xe VII; [e] in our spectra, we also identified the transitions to the levels $5s5p\ ^3P^\circ_{0,1}$ but these lines were too weak for a reliable measurement.

was a 1 m radius concave grating with 1200 l/mm grating blazed at 2° 45′ (corresponding to 65 nm in our case). The grating was coated with Pt in order to optimize the reflectivity in the UV region.

Depending on the ion beam energy, different ions in their excited states can be produced by the BF interaction. In order to optimize the number of ions in the ionization states of interest for the present work, an ion beam of 1.7 MeV was chosen for the measurements in agreement with the model proposed in [58].

The light was detected by a thin, back-illuminated, liquid nitrogen-cooled CCD detector specially developed for far UV measurements. The CCD detector is based on a EEV CCD15-1 chip of 27.6×6.9 mm (1024×256) [59,60]. The CCD, which replaces the exit slit of the spectrometer, was tilted to an angle of 125° relatively to the spectrometer exit arm axis in order to be tangential to the Rowland circle. Under that geometry, it has a dispersion of 0.02 nm/pixel and detects light over a ≈20 nm wide region with a fairly constant resolution giving a line width (*FWHM*) of ∼0.12 nm. The whole system was working under vacuum (10^{-5} Torr). The CCD images were transferred to a networked computer and analyzed by a dedicated software. The XY image was transformed by binning the horizontal lines into a file containing a list of numbers representing the line intensities as a function of the wavelength.

For the decay curve measurements, the spectra have been recorded at different foil positions along the ion beam path. The foil holder was automatically moved to several different positions and its position measured by a digital gauge (Mitutoyo 5 MQ65-5P) with a resolution of 10 μm. The spectra were recorded at least at 15 different foil positions. Since the stability of the foil position can influence the lifetime estimation, it has been regularly checked. The lifetime measurements performed by the BFS are also sensitive to variations in the ion beam intensity. In order to avoid this problem the light measurements were normalized to a fixed beam flux entering the electrically isolated excitation chamber. The current was measured with an Ortec 439 current digitizer.

Table 5. Weighted oscillator strengths ($\log gf$) and transition probabilities (gA) as obtained using the $HFR+CP$ method for Xe VII lines. Only transitions for which $\log gf \geq -1.0$ are listed.

λ (nm)*	Transition	$\log gf$	gA (s^{-1})
36.6168a	$5s5p\,{}^1P^\circ_1$–$4f5p\,{}^1D_2$	−0.847	7.11(9)
38.6560a	$5s5p\,{}^3P^\circ_0$–$5s6s\,{}^3S_1$	−0.695	9.00(9)
39.3114a	$5s5p\,{}^3P^\circ_1$–$5s6s\,{}^3S_1$	−0.242	2.47(10)
39.3919a	$5p^2\,{}^1D_2$–$5p6s\,{}^1P^\circ_1$	−0.365	1.85(10)
39.8804	$5p^2\,{}^3P_1$–$5p6s\,{}^3P^\circ_2$	−0.349	1.87(10)
40.1067	$5p^2\,{}^1D_2$–$5p6s\,{}^3P^\circ_2$	−0.347	1.86(10)
40.4635a	$5p^2\,{}^3P_0$–$5p6s\,{}^3P^\circ_1$	−0.434	1.50(10)
41.4666a	$5s5p\,{}^3P^\circ_2$–$5s6s\,{}^3S_1$	−0.028	3.64(10)
41.9989a	$5p^2\,{}^3P_2$–$5p6s\,{}^1P^\circ_1$	−0.249	2.14(10)
42.3513	$5p^2\,{}^3P_1$–$5p6s\,{}^3P^\circ_1$	−0.711	7.21(9)
42.6072a	$5p^2\,{}^1D_2$–$5p6s\,{}^3P^\circ_1$	−0.315	1.78(10)
42.7183a	$5p^2\,{}^3P_1$–$5p6s\,{}^3P^\circ_0$	−0.501	1.15(10)
42.8115	$5p^2\,{}^3P_2$–$5p6s\,{}^3P^\circ_2$	−0.096	2.92(10)
45.7851a	$5s5p\,{}^1P^\circ_1$–$5s6s\,{}^1S_0$	−0.249	1.79(10)
46.1363	$5p^2\,{}^1S_0$–$5p6s\,{}^1P^\circ_1$	−0.319	1.50(10)
48.2877a	$5s5p\,{}^3P^\circ_1$–$5p5d\,{}^1D_2$	−0.964	3.11(9)
49.4243a	$5p^2\,{}^1D_2$–$5p5d\,{}^1F^\circ_3$	0.254	4.86(10)
52.1832a	$5s5p\,{}^3P^\circ_0$–$5s5d\,{}^3D_1$	0.024	2.59(10)
52.4799	$5p^2\,{}^3P_1$–$5p5d\,{}^3P^\circ_2$	−0.452	8.52(9)
52.6644a	$5p^2\,{}^3P_1$–$5p5d\,{}^3P^\circ_1$	0.087	2.93(10)
52.7697a	$5p^2\,{}^3P_1$–$5p5d\,{}^3P^\circ_0$	−0.235	1.39(10)
52.8720a	$5p^2\,{}^1D_2$–$5p5d\,{}^3P^\circ_2$	−0.202	1.50(10)
53.0597	$5p^2\,{}^1D_2$–$5p5d\,{}^3P^\circ_1$	−0.570	6.37(9)
53.1179a	$5s5p\,{}^3P^\circ_1$–$5p5d\,{}^3D_2$	0.364	5.47(10)
53.3763a	$5p^2\,{}^3P_0$–$5p5d\,{}^3D^\circ_1$	0.290	4.58(10)
53.3850a	$5s5p\,{}^3P^\circ_1$–$5p5d\,{}^3D_1$	−0.127	1.75(10)
53.4966a	$5p^2\,{}^1D_2$–$5p5d\,{}^3D^\circ_3$	0.510	7.54(10)
53.5980a	$5p^2\,{}^3P_2$–$5p5d\,{}^1F^\circ_3$	0.436	6.30(10)
54.3102a	$5p^2\,{}^3P_0$–$5s6p\,{}^1P^\circ_1$	−0.727	4.25(9)
54.7780a	$5p^2\,{}^3P_1$–$5p5d\,{}^3D^\circ_2$	0.405	5.64(10)
54.8201	$5s5d\,{}^1D_2$–$5p6s\,{}^1P^\circ_1$	−0.238	1.28(10)
55.2059	$5p^2\,{}^1D_2$–$5p5d\,{}^3D^\circ_2$	−0.243	1.25(10)
56.6050a	$5s5p\,{}^3P^\circ_2$–$5p5d\,{}^3D_3$	0.610	8.48(10)
56.7096	$5p2\,{}^3P_1$–$5p5d\,{}^3D^\circ_1$	−0.456	7.23(9)
57.1309a	$5s5p\,{}^3P^\circ_2$–$5p5d\,{}^3D_2$	−0.131	1.51(10)
57.1656a	$5s5d\,{}^3D_1$–$5s5f\,{}^3F^\circ_2$	0.535	6.98(10)
57.4451a	$5s5d\,{}^3D_2$–$5s5f\,{}^3F^\circ_3$	0.707	1.03(11)
57.4746	$5s5d\,{}^3D_2$–$5s5f\,{}^3F^\circ_2$	−0.218	1.22(10)
57.5831	$5p2\,{}^3P_1$–$5s6p\,{}^3P^\circ_2$	−0.708	3.92(9)
57.6768a	$5p2\,{}^3P_2$–$5p5d\,{}^3P^\circ_2$	0.387	4.91(10)
57.8640a	$5s5d\,{}^3D_3$–$5s5f\,{}^3F^\circ_4$	0.872	1.48(11)
57.8992	$5p2\,{}^3P_2$–$5p5d\,{}^3P^\circ_1$	−0.334	9.24(9)
57.9875	$5s5d\,{}^3D_3$–$5s5f\,{}^3F^\circ_3$	−0.222	1.19(10)
58.0549a	$5p2\,{}^1D_2$–$5s6p\,{}^3P^\circ_2$	−0.425	7.42(9)
58.2404	$5p2\,{}^1D_2$–$5s6p\,{}^1P^\circ_1$	−0.675	4.16(9)
58.4196a	$5p2\,{}^3P_2$–$5p5d\,{}^3D^\circ_3$	0.419	5.15(10)
58.8717a	$5p2\,{}^3P_1$–$5p5d\,{}^1D^\circ_2$	−0.008	1.89(10)
59.3655	$5p2\,{}^1D_2$–$5p5d\,{}^1D^\circ_2$	−0.062	1.64(10)
59.4643a	$5p2\,{}^1S_0$–$5p5d\,{}^1P^\circ_1$	0.270	3.52(10)
60.4642	$5p2\,{}^3P_2$–$5p5d\,{}^3D^\circ_2$	−0.655	4.06(9)
60.4913a	$5p2\,{}^1D_2$–$5p5d\,{}^3F^\circ_3$	−0.409	7.10(9)
60.8706a	$5s5p\,{}^1P^\circ_1$–$5p5d\,{}^1D_2$	0.691	8.84(10)
61.2509	$5s5d\,{}^1D_2$–$5p6s\,{}^3P^\circ_1$	−0.835	2.60(9)
62.4383a	$5s5d\,{}^1D_2$–$5s5f\,{}^1F^\circ_3$	0.908	1.38(11)
63.4144a	$5p2\,{}^1D_2$–$5p5d\,{}^3F^\circ_2$	−0.396	6.64(9)
63.9002	$5p2\,{}^3P_2$–$5s6p\,{}^3P^\circ_2$	−0.828	2.44(9)
64.1235	$5p2\,{}^3P_2$–$5s6p\,{}^1P^\circ_1$	−0.664	3.53(9)
66.0502a	$5s5p\,{}^3P^\circ_1$–$5p2\,{}^3P_2$	−0.419	5.81(9)
67.528a	$5s5d\,{}^3D_3$–$5p5d\,{}^1F^\circ_3$	−0.843	2.08(9)
69.6646	$4f5s\,{}^3F^\circ_3$–$4f5p\,{}^1D_2$	−0.786	2.27(9)
69.8038a	$5s^2\,{}^1S_0$–$5s5p\,{}^1P^\circ_1$	0.186	2.10(10)
72.0778	$4f5s\,{}^3F^\circ_3$–$4f5p\,{}^1G_4$	−0.889	1.64(9)
72.1800a	$5s5p\,{}^3P^\circ_0$–$5p2\,{}^3P_1$	−0.264	7.00(9)
72.3034	$4f5s\,{}^3F^\circ_4$–$4f5p\,{}^1G_4$	−0.713	2.45(9)
72.3701a	$5s5p\,{}^3P^\circ_2$–$5p2\,{}^3P_2$	0.117	1.66(10)
72.7474	$5s5d\,{}^3D_1$–$5p5d\,{}^3P^\circ_2$	−0.739	2.30(9)
72.9531a	$4f5s\,{}^1F^\circ_3$–$4f5p\,{}^1D_2$	0.179	1.91(10)
73.1028a	$5s5d\,{}^3D_1$–$5p5d\,{}^3P^\circ_1$	−0.173	8.38(9)
73.2518a	$5s5d\,{}^3D_2$–$5p5d\,{}^3P^\circ_2$	−0.003	1.23(10)
73.3052	$5s5d\,{}^3D_1$–$5p5d\,{}^3P^\circ_0$	−0.474	4.17(9)
73.4291a	$4f5s\,{}^3F^\circ_2$–$4f5p\,{}^3D_1$	−0.013	1.20(10)
73.6079	$5s5d\,{}^3D_2$–$5p5d\,{}^3P^\circ_1$	−0.515	3.75(9)
73.7206a	$5s5p\,{}^3P^\circ_1$–$5p2\,{}^1D_2$	−0.441	4.46(9)
74.0061	$5s6s\,{}^3S_1$–$5p6s\,{}^1P^\circ_1$	−0.792	1.97(9)
74.1323	$5s5d\,{}^3D_3$–$5p5d\,{}^3P^\circ_2$	−0.394	4.90(9)
74.4513	$5s5d\,{}^3D_2$–$5p5d\,{}^3D^\circ_3$	−0.309	5.92(9)
74.4961a	$5s5p\,{}^3P^\circ_1$–$5p2\,{}^3P_1$	−0.418	4.61(9)
74.7194	$5s5d\,{}^1D_2$–$5p5d\,{}^1P^\circ_1$	−0.276	6.34(9)
74.7607a	$4f5s\,{}^3F^\circ_2$–$4f5p\,{}^3D_2$	−0.149	8.50(9)
74.8890a	$4f5s\,{}^3F^\circ_3$–$4f5p\,{}^3D_2$	−0.088	9.72(9)
75.3652a	$5s5d\,{}^3D_3$–$5p5d\,{}^3D^\circ_3$	0.066	1.37(10)
75.6035a	$4f5s\,{}^1F^\circ_3$–$4f5p\,{}^1G_4$	0.203	1.84(10)
75.6620a	$4f5s\,{}^3F^\circ_3$–$4f5p\,{}^3D_3$	−0.097	9.33(9)
75.9107a	$4f5s\,{}^3F^\circ_4$–$4f5p\,{}^3D_3$	0.044	1.28(10)
76.405a	$5s5d\,{}^1D_2$–$5p5d\,{}^1F^\circ_3$	0.283	2.17(10)
76.5684a	$5s6s\,{}^3S_1$–$5p6s\,{}^3P^\circ_2$	0.162	1.65(10)
76.9534a	$5s5p\,{}^1P^\circ_1$–$5p2\,{}^1S_0$	−0.249	6.35(9)
77.2392	$5s5d\,{}^3D_1$–$5p5d\,{}^3D^\circ_2$	−0.713	2.17(9)
77.9119a	$4f5s\,{}^3F^\circ_4$–$4f5p\,{}^3G_5$	0.416	2.85(10)
77.9508	$5s6s\,{}^1S_0$–$5p6s\,{}^1P^\circ_1$	−0.034	1.01(10)
78.6329a	$4f5s\,{}^3F^\circ_3$–$4f5p\,{}^3F_4$	0.176	1.61(10)
78.8022	$5s5d\,{}^3D_3$–$5p5d\,{}^3D^\circ_2$	−0.096	8.62(9)
78.8991a	$4f5s\,{}^3F^\circ_4$–$4f5p\,{}^3F_4$	−0.046	9.64(9)
79.5564	$4f5s\,{}^1F^\circ_3$–$4f5p\,{}^3D_3$	−0.667	2.27(9)
79.7156a	$4f5s\,{}^3F^\circ_2$–$4f5p\,{}^1F_3$	−0.071	8.94(9)
79.8626	$4f5s\,{}^3F^\circ_3$–$4f5p\,{}^1F_3$	−0.568	2.83(9)
80.1398	$4f5s\,{}^3F^\circ_4$–$4f5p\,{}^1F_3$	−0.998	1.05(9)
81.1544a	$5s5p\,{}^3P^\circ_1$–$5p2\,{}^3P_0$	−0.321	4.83(9)
81.6825a	$5s5p\,{}^3P^\circ_2$–$5p2\,{}^1D_2$	−0.209	6.19(9)
81.7595	$5s5d\,{}^3D_2$–$5p5d\,{}^3D^\circ_1$	−0.133	7.35(9)
81.8149a	$5s5d\,{}^3D_3$–$5p5d\,{}^3F^\circ_4$	0.143	1.38(10)
82.6386a	$5s5p\,{}^3P^\circ_2$–$5p2\,{}^3P_1$	−0.230	5.78(9)
83.3125	$5s5d\,{}^3D_1$–$5s6p\,{}^1P^\circ_1$	−0.935	1.12(9)
83.5876	$5s5d\,{}^3D_2$–$5s6p\,{}^3P^\circ_2$	−0.930	1.12(9)
84.2136a	$4f5s\,{}^1F^\circ_3$–$4f5p\,{}^1F_3$	−0.171	6.37(9)
84.7421a	$5s5d\,{}^3D_3$–$5s6p\,{}^3P^\circ_2$	0.272	1.74(10)
86.2277	$5s6s\,{}^3S_1$–$5p6s\,{}^3P^\circ_1$	−0.182	5.89(9)
86.3285a	$5s5d\,{}^3D_2$–$5p5d\,{}^1D^\circ_2$	−0.684	1.86(9)
87.5422a	$4f5s\,{}^3F^\circ_2$–$4f5p\,{}^3F_2$	−0.149	6.20(9)
87.7201	$4f5s\,{}^3F^\circ_3$–$4f5p\,{}^3F_2$	−0.270	4.67(9)
87.7624	$5s6s\,{}^3S_1$–$5p6s\,{}^3P^\circ_0$	−0.582	2.27(9)
88.2137a	$4f5s\,{}^3F^\circ_3$–$4f5p\,{}^3G_4$	−0.328	4.02(9)
88.4002a	$5s5d\,{}^3D_1$–$5s6p\,{}^3P^\circ_1$	−0.648	1.93(9)
88.5528a	$4f5s\,{}^3F^\circ_4$–$4f5p\,{}^3G_4$	0.129	1.14(10)
88.5787a	$5s5d\,{}^3D_1$–$5s6p\,{}^3P^\circ_0$	−0.443	3.06(9)

Table 5. *Continued.*

λ (nm)*	Transition	log gf	gA (s^{-1})
88.7300a	$5s5d\,{}^3D_2-5p5d\,{}^3F^{\circ}_3$	−0.169	5.74(9)
88.8024a	$4f5s\,{}^3F^{\circ}_3-4f5p\,{}^3F_3$	−0.313	4.13(9)
89.1443a	$5s5d\,{}^3D_2-5s6p\,{}^3P^{\circ}_1$	−0.225	5.01(9)
89.1443a	$4f5s\,{}^3F^{\circ}_4-4f5p\,{}^3F_3$	−0.064	7.27(9)
90.0309	$5s5d\,{}^3D_3-5p5d\,{}^3F^{\circ}_3$	−0.420	3.13(9)
91.0956a	$4f5s\,{}^3F^{\circ}_2-4f5p\,{}^3G_3$	−0.190	5.17(9)
91.2875	$4f5s\,{}^3F^{\circ}_3-4f5p\,{}^3G_3$	−0.435	2.92(9)
91.6305	$5s6s\,{}^1S_0-5p6s\,{}^3P^{\circ}_1$	−0.665	1.72(9)
92.0870a	$5s5p\,{}^1P^{\circ}_1-5p2\,{}^3P_2$	-0.676	1.65(9)
93.5541	$4f5s\,{}^1F^{\circ}_3-4f5p\,{}^3G_4$	−0.718	1.46(9)
94.2152	$4f5s\,{}^1F^{\circ}_3-4f5p\,{}^3F_3$	−0.323	3.58(9)
94.3220a	$5s5d\,{}^3D_1-5p5d\,{}^3F^{\circ}_2$	−0.325	3.54(9)
95.1656	$5s5d\,{}^3D_2-5p5d\,{}^3F^{\circ}_2$	−0.735	1.35(9)
97.0170a	$4f5s\,{}^1F^{\circ}_3-4f5p\,{}^3G_3$	−0.266	3.82(9)
99.7406a	$5s5d\,{}^1D_2-5s6p\,{}^1P^{\circ}_1$	−0.119	5.10(9)
107.1226	$5s5d\,{}^1D_2-5s6p\,{}^3P^{\circ}_1$	−0.806	9.11(8)
107.7120a	$5s5p\,{}^1P^{\circ}_1-5p2\,{}^1D_2$	−0.555	1.61(9)
132.7545	$5s6p\,{}^3P^{\circ}_1-5s6d\,{}^3D_2$	0.401	9.50(9)
132.7598	$5s6p\,{}^3P^{\circ}_0-5s6d\,{}^3D_1$	0.103	4.78(9)
133.163a	$5s6p\,{}^3P^{\circ}_1-5s6d\,{}^3D_1$	−0.162	2.57(9)
133.6773	$5p5d\,{}^3F^{\circ}_3-5s6d\,{}^3D_2$	−0.918	4.52(8)
138.4045	$5p5d\,{}^1D^{\circ}_2-5s6d\,{}^3D_3$	0.130	4.71(9)
139.5245	$5p5d\,{}^1D^{\circ}_2-5s6d\,{}^3D_2$	−0.678	7.17(8)
146.095a	$5s6p\,{}^3P^{\circ}_2-5s6d\,{}^3D_3$	0.576	1.19(10)
146.1604	$5s6p\,{}^1P^{\circ}_1-5s6d\,{}^3D_2$	−0.532	9.17(8)
146.6534	$5s6p\,{}^1P^{\circ}_1-5s6d\,{}^3D_1$	−0.726	5.78(8)
147.325a	$5s6p\,{}^3P^{\circ}_2-5s6d\,{}^3D_2$	−0.183	2.02(9)
153.3789	$5p5d\,{}^3D^{\circ}_1-5s6d\,{}^3D_2$	−0.975	3.00(8)
155.6832	$5p5d\,{}^3F^{\circ}_4-5s6d\,{}^3D_3$	−0.719	5.32(8)
186.8670	$5s6s\,{}^3S_1-5s6p\,{}^3P^{\circ}_2$	0.198	3.01(9)
188.7897	$5s6s\,{}^3S_1-5s6p\,{}^1P^{\circ}_1$	−0.642	4.27(8)
194.7685	$4f5p\,{}^1D_2-5s5f\,{}^1F^{\circ}_3$	−0.672	3.67(8)
201.0815	$5s6s\,{}^3S_1-5p5d\,{}^1D^{\circ}_2$	−0.314	8.05(8)
216.7060	$5s6s\,{}^1S_0-5s6p\,{}^1P^{\circ}_1$	−0.197	9.02(8)
217.0400	$5s6s\,{}^3S_1-5s6p\,{}^3P^{\circ}_1$	−0.076	1.20(9)
218.1151	$5s6s\,{}^3S_1-5s6p\,{}^3P^{\circ}_0$	−0.441	5.04(8)
231.5068	$5p2\,{}^1D_2-4f5s\,{}^1F^{\circ}_3$	−0.884	1.61(8)
254.8824	$5s6s\,{}^1S_0-5s6p\,{}^3P^{\circ}_1$	−0.711	2.01(8)
371.9595	$4f5p\,{}^1G_4-5p5d\,{}^1F^{\circ}_3$	−0.488	1.56(8)
399.5832	$4f5p\,{}^1D_2-5p5d\,{}^1P^{\circ}_1$	−0.912	4.97(7)
412.9189	$4f5p\,{}^3F_2-5p5d\,{}^3D^{\circ}_1$	−0.932	4.51(7)
433.8869	$4f5p\,{}^3F_4-5p5d\,{}^3D^{\circ}_3$	−0.687	7.36(7)
493.5675	$4f5p\,{}^3D_3-5p5d\,{}^3P^{\circ}_2$	−0.825	4.08(7)
520.3360	$4f5p\,{}^1F_3-5p5d\,{}^3D^{\circ}_2$	−0.858	3.38(7)
522.7029	$4f5p\,{}^3F_3-5p5d\,{}^1D^{\circ}_2$	−0.911	2.99(7)
584.8042	$4f5s\,{}^3F^{\circ}_4-5s5d\,{}^3D_3$	−0.657	4.30(7)
628.7569	$4f5s\,{}^3F^{\circ}_3-5p5d\,{}^3D_2$	−0.848	2.39(7)
655.9437	$4f5p\,{}^3G_4-5p5d\,{}^3F^{\circ}_3$	−0.683	3.24(7)
713.6301	$5s5f\,{}^3F^{\circ}_3-5s6d\,{}^3D_3$	−0.976	1.42(7)
732.8822	$5s5f\,{}^3F^{\circ}_4-5s6d\,{}^3D_3$	0.075	1.53(8)
744.4520	$5s5f\,{}^3F^{\circ}_3-5s6d\,{}^3D_2$	−0.108	9.37(7)
752.3515	$5s5f\,{}^3F^{\circ}_2-5s6d\,{}^3D_1$	−0.284	5.96(7)
874.1915	$4f5p\,{}^3G_3-5p5d\,{}^3F^{\circ}_2$	−0.864	1.21(7)
911.1608	$4f5p\,{}^3G_5-5p5d\,{}^3F^{\circ}_4$	−0.613	1.98(7)

* Wavelengths are given in vacuum (in air) below (above) 200.0 nm. The observed wavelengths are taken from [19] (a) or otherwise calculated from the available experimental energy levels [13,18,19].

Table 6. Oscillator strengths (log gf) and transition probabilities (gA) as obtained using the *HFR + CP* method for Xe VIII lines. Only transitions for which log $gf \geq -1.0$ are listed.

λ (nm)*	Transition	log gf	gA (s^{-1})
22.1841a	$5s_{1/2}-6p^0_{3/2}$	−0.994	1.37(10)
25.532a	$4f^0_{5/2}-6g_{7/2}$	−0.106	8.02(10)
25.568a	$4f^0_{7/2}-6g_{9/2}$	0.006	1.04(11)
32.625b	$5d_{3/2}-6f^0_{5/2}$	−0.489	2.03(10)
32.781b	$4f^0_{5/2}-5g_{7/2}$	0.327	1.32(11)
32.841b	$4f^0_{7/2}-5g_{9/2}$	0.439	1.70(11)
32.915b	$5d_{5/2}-6f^0_{7/2}$	−0.338	2.83(10)
35.841b	$5p^0_{1/2}-6s_{1/2}$	−0.400	2.07(10)
38.399b	$5p^0_{3/2}-6s_{1/2}$	−0.129	3.36(10)
51.7007a	$5p^0_{1/2}-5d_{3/2}$	0.325	5.28(10)
53.279b	$5d_{3/2}-5f^0_{5/2}$	0.643	1.03(11)
54.000b	$5d_{5/2}-5f^0_{7/2}$	0.792	1.42(11)
54.129a	$5d_{5/2}-5f^0_{5/2}$	−0.510	7.04(9)
56.2547a	$5p^0_{3/2}-5d_{5/2}$	0.544	7.37(10)
57.1894a	$5p^0_{3/2}-5d_{3/2}$	−0.418	7.79(9)
62.7959	$5f^0_{5/2}-6g_{7/2}$	−0.523	5.07(9)
62.9624	$5f^0_{7/2}-6g_{9/2}$	−0.412	6.52(9)
70.99a	$5d_{3/2}-6p^0_{3/2}$	−0.710	2.58(9)
72.489b	$5d_{5/2}-6p^0_{3/2}$	0.235	2.18(10)
74.0458a	$5s_{1/2}-5p^0_{3/2}$	0.031	1.31(10)
74.92a	$5d_{3/2}-6p^0_{1/2}$	−0.034	1.10(10)
85.8607a	$5s_{1/2}-5p^0_{1/2}$	−0.334	4.19(9)
112.366b	$6d_{3/2}-6f^0_{5/2}$	0.743	2.92(10)
112.385b	$5g_{7/2}-6h^0_{9/2}$	1.101	6.66(10)
112.396b	$5g_{9/2}-6h^0_{11/2}$	1.190	8.17(10)
112.4025	$5g_{9/2}-6h^0_{9/2}$	−0.543	1.51(9)
113.8110	$6d_{5/2}-6f^0_{7/2}$	0.893	4.03(10)
114.110b	$6d_{5/2}-6f^0_{5/2}$	−0.411	1.99(9)
119.00a	$6p^0_{1/2}-6d_{3/2}$	0.488	1.45(10)
128.175b	$6p^0_{3/2}-6d_{5/2}$	0.711	2.09(10)
130.46a	$6p^0_{3/2}-6d_{3/2}$	−0.251	2.20(9)
137.661b	$5f^0_{5/2}-5g_{7/2}$	0.808	2.27(10)
138.41a	$5f^0_{7/2}-5g_{9/2}$	0.918	2.88(10)
138.4447	$5f^0_{7/2}-5g_{7/2}$	−0.626	8.24(8)
180.898b	$6s_{1/2}-6p^0_{3/2}$	0.256	3.67(9)
208.761b	$6s_{1/2}-6g^0_{1/2}$	−0.107	1.19(9)
212.404b	$4f^0_{7/2}-5d_{5/2}$	−0.265	8.05(8)
215.4123	$5g_{9/2}-6f^0_{7/2}$	0.185	2.20(9)
216.4151	$5g_{7/2}-6f^0_{5/2}$	0.069	1.66(9)
223.572b	$4f^0_{5/2}-5d_{3/2}$	−0.442	4.82(8)
247.387b	$6f^0_{5/2}-6g_{7/2}$	0.984	1.06(10)
248.801b	$6f^0_{7/2}-6g_{7/2}$	−0.451	3.82(8)
248.867b	$6f^0_{7/2}-6g_{9/2}$	1.093	1.34(10)
324.698b	$5f^0_{7/2}-6d_{5/2}$	0.282	1.21(9)
335.003b	$5f^0_{5/2}-6d_{3/2}$	0.114	7.72(8)

* Wavelengths are given in vacuum (in air) below (above) 200.0 nm. The observed wavelengths are taken from [19] (a), from [32] (b) or otherwise calculated from the available experimental energy levels [18,19].

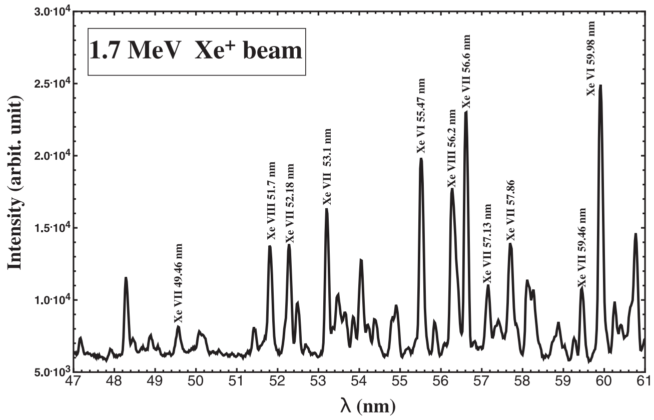

Fig. 1. BFS xenon spectrum between 48 and 60 nm registered at an energy of 1.7 MeV. The strongest Xe VI, Xe VII and Xe VIII lines are identified.

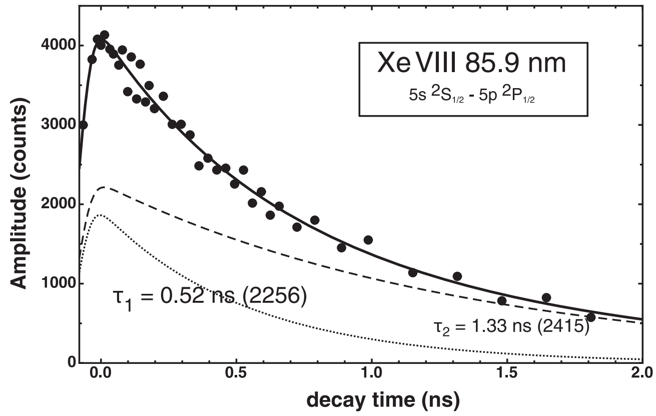

Fig. 2. Decay curve of the $5s\ ^2S_{1/2}$–$5p\ ^2P^{\circ}_{3/2}$ Xe VIII transition observed at 85.9 nm. This curve can be decomposed in a primary and a secondary contribution whose lifetime values are indicated on the figure. The numbers between parentheses are related to the amplitudes of these two components.

The lines observed ($35 < \lambda < 95$ nm) were identified by using recent analyses or compilations [13,19,44]. A section of a xenon spectrum, recorded between 47 and 61 nm at an energy of 1.7 MeV, is shown in Figure 1. Some transitions of Xe VI, Xe VII and Xe VIII are indicated on the figure. From the recorded CCD data, the profiles of the lines were fitted with a Gaussian in order to subtract the background. Repeating the fitting procedure for different foil positions allows to obtain a decay curve. One example of a decay curve, recorded during the present experimental investigation, is illustrated in Figure 2. It shows the intensity of the emitted light as a function of time in the case of the Xe VIII transition at 85.9 nm. Here it should be mentioned that the distance-to-time conversion was obtained using an ion beam velocity of 1.51 mm/ns.

The lifetimes measured in the present work are reported in Table 4 (Col. 7). Radiative lifetimes have been measured for 12 levels of Xe VII belonging to the configurations $5s5p$, $5p^2$, $5s5d$, $5s6s$, $5p5d$, $4f5p$, $5s5f$ and for 4 levels of the $5p$ and $5d$ configurations of Xe VIII. Each result is the mean value of at least five repeated measurements. The uncertainties are quoted as twice the standard deviation of the mean. The beam-foil measurements are affected by cascading problems due to non-selective excitation in the carbon foil that distorts the decay curves which appear as multiexponential decays. In order to deal with this effect, the data were fitted with a model describing the whole decay curve as a growing part followed by a multi-exponential decay. The estimated lifetime of the investigated level in this case corresponds to the main contribution to the decay curve.

In the last column of Table 4, we give the depopulation channels which have been used for the measurements. Some comments concerning possible blends are indicated as footnotes to the table.

The experimental values are compared with the HFR + CP and with the MCDF theoretical values in Table 4. The agreement is very good except for the two $5d$ $^2D^{\circ}_{3/2,5/2}$ levels of Xe VIII.

For the $5s5d\ ^3D_{1,2,3}$ and $5s5f\ ^3F_4$ levels of Xe VII the direct multi-exponential fitting procedure leaded to large discrepancies between theory and experiment because for those levels, the lifetimes (estimated from the calculations) of some of the most probable cascading levels are close or slightly longer that the lifetime of the level itself. In such a situation, is is well-known that a careless fit could lead to meaningless results because the numerical system is extremely ill conditioned [62]. For these levels, we have adopted a constrained fitting procedure where we imposed to the model a set of cascade lifetimes close to the theoretical ones. Only the amplitudes of the different components were left free. This approach, conceptually similar to the ANDC technique [61], but where decay curves of the cascading levels are simulated, avoids the pitfall of the free fits. In each case, it was possible to obtain a decay curve that nicely reproduces the observed patterns. This confirms that the experimental observations are in agreement with the proposed theoretical lifetime values. The lifetime values quoted in the table were obtained by fitting the decay curves with a function where only the amplitudes of all components and the lifetime of the main component was left free whereas the cascading lifetimes were fixed to the theoretical values. The selection of the components to include in the analysis was based on the experimentally observed intensities [13,18,19] and we restricted the summation to the levels having a strong decay channel to the studied level. For these four levels, the results presented in Table 4 were obtained using this constrained fitting procedure.

In Xe VIII, the lifetime of the four strongest lines appearing in our spectra have been measured. For the $5p$ $^2P^{\circ}$ term, the agreement between experiment and theory is good, whereas for the $5d\ ^2D_{3/2,5/2}$ levels both experimental values are 40% larger than the predictions. For these two decay curves, a constrained fit, including the main cascades [from the $5f\ ^2F^{\circ}$ ($\simeq$0.06 ns), $6f\ ^2F^{\circ}$, $6p$ $^2P^{\circ}$ ($\simeq$0.11 ns) and $7p\ ^2P^{\circ}$ ($\simeq$0.12 ns) terms] was not compatible with the observational data and, consequently, the values presented in Table 4 were deduced from direct fits. The difficulty is thus arising here from the experiment and is related to the fact that it appeared impossible to disentangle from the decay curves the different components with similar lifetime values.

Weighted oscillator strengths ($\log gf$) and transition probabilities (gA) have been calculated for a number of transitions of Xe VII and Xe VIII involving low-lying levels. These results are reported in Tables 5 and 6. Only the transitions for which $\log gf > -1.0$ are listed in the tables.

7 Conclusions

Radiative lifetimes have been obtained for 12 levels belonging to the configurations $5s5p$, $5p^2$, $5s5d$, $5s6s$, $5p5d$, $4f5p$, $5p5d$ of Xe VII and for 4 levels of the $5p$ and $5d$ configurations of Xe VIII. Core-polarization effects have been included in the framework of a relativistic Hartree-Fock approach. The HFR results have been compared with the entirely relativistic MCDF calculations carried out for the same levels. The accuracy of the theoretical data has been assessed through comparisons with radiative lifetime measurements performed with the BF spectroscopy. A good agreement between theory and experiment has generally been observed after a careful analysis of the cascades. A new set of transition probabilities is proposed for 169 transitions of Xe VII and 45 transitions of Xe VIII.

A limitation to the accuracy of the results reported in Tables 5 and 6 might possibly originate from cancellation effects affecting the line strengths. In fact, this is not the case because, for all the transitions quoted in the tables, it was verified that the cancellation factor, as defined in reference [46], is larger than 0.01 for all the depopulating channels indicating that such effects were not present.

For the different reasons outlined above, we are confident in the accuracy of the gf values reported in Tables 5 and 6 which extend the data available for these two ions.

Financial support from the Belgian Institut Interuniversitaire des Sciences Nucléaires (IISN) and from the FNRS is acknowledged. Three of us (E.B., P.P. and P.Q.) are respectively Research Director and Research Associates of this organization. V. Fivet has a FRIA fellowship.

References

1. D. Péquignot, J.-P. Baluteau, Astron. Astrophys. **283**, 593 (1994)
2. T. Schöning, K. Butler, Astron. Astrophys. Suppl. **128**, 581 (1998)
3. H. Sobral, M. Raineri, D. Schinca, M. Gallardo, R. Duchowicz, IEEE J. Quantum Electron. **35**, 1308 (1999)
4. É. Biémont, P. Quinet, C. Zeippen, Phys. Scr. **71**, 163 (2005)
5. É. Biémont, V. Buchard, H.-P. Garnir, P.-H. Lefèbvre, P. Quinet, Eur. Phys. J. D **33**, 181 (2005)
6. B.C. Fawcett, B.B. Jones, R. Wilson, Proc. Phys. Soc. A **78**, 1223 (1961)
7. J.A. Kernahan, E.H. Pinnington, J.A. O'Neill, J.L. Bahr, K.E. Donelly, J. Opt. Soc. Am. **70**, 1126 (1980)
8. E.J. Knystautas, J. Sugar, J. Roberts, J. Opt. Soc. Am. **69**, 172 (1979)
9. E.H. Pinnington, J.A. Kernahan, W. Ansbacher, A. Tauheed, J. Opt. Soc. Am. B **8**, 2233 (1991)
10. E.H. Pinnington, W. Ansbacher, J.A. Kernahan, J. Opt. Soc. Am. B **4**, 696 (1987)
11. V. Kaufman, J. Sugar, J. Opt. Soc. Am. B **4**, 1919 (1987)
12. M. Wang, A. Arnesen, R. Hallin, F. Heijkenskjöld, M.O. Larsson, A. Wännström, A.G. Trigueiros, A.V. Loginov, J. Opt. Soc. Am. B **14**, 3277 (1997)
13. S.S. Churilov, Y.N. Joshi, Phys. Scr. **65**, 35 (2002)
14. R. Hallin, J.A. Leavitt, A. Lindgård, P.W. Rathmann, H. Vach, E. Veje, Nucl. Instrum. Meth. Phys. Res. A **202**, 42 (1982)
15. J. Blackburn, P.K. Carrol, J. Costello, G. O'Sullivan, J. Opt. Soc. Am. **73**, 1325 (1983)
16. M.O. Larsson, A.M. Gonzalez, R. Hallin, R. Heijkenskjöld, R. Hutton, A. Langereis, B. Nyström, G.O'Sullivan, A. Wännström, Phys. Scr. **51**, 69 (1995)
17. G.H. Cavalcanti, F.R.T. Luna, A.G. Trigueiros, F. Bredice, H. Sobral, R. Hutton, M. Wang, J. Opt. Soc. Am. B **14**, 2459 (1997)
18. `http://physics.nist.gov/PhysRefData/ASD/index.html`
19. E.B. Saloman, J. Phys. Chem. Ref. Data **33**, 765 (2004)
20. A. Hibbert, Nucl. Instrum. Methods **202**, 323 (1982)
21. J. Migdalek, A. Bojara, J. Phys. B **21**, 2221 (1988)
22. J. Migdalek, W.E. Baylis, J. Phys. B **19**, 1 (1986)
23. L. Glowacki, J. Migdalek, J. Phys. B **36**, 3629 (2003)
24. H.-S. Chou, K.-N. Huang, Phys. Rev. A **46**, 3725 (1992)
25. H.-S. Chou, H.-C. Chi, K.-N. Huang, Phys. Rev. A **48**, 2453 (1993)
26. É. Biémont, C. Froese Fischer, M.R. Godefroid, P. Palmeri, P. Quinet, Phys. Rev. A **62**, 032512 (2000)
27. C. Lavin, I. Martin, J. Quant. Spectrosc. Radiat. Transfer **52**, 21 (1994)
28. C. Lavin, P. Martin, I. Martin, J. Karwowski, Int. J. Quantum Chem. Symp. **27**, 385 (1993)
29. L.J. Curtis, R. Matulioniene, D.G. Ellis, C. Froese Fischer, Phys. Rev. A **62**, 052513 (2000)
30. E.H. Pinnington, R.N. Gosselin, J.A. O'Neill, J.A. Kernahan, K.E. Donnelly, R.L. Brooks, Phys. Scr. **20**, 151 (1979)
31. M. Wang, A. Arnesen, R. Hallin, F. Heijkenskjöld, A. Langereis, M.O. Larsson, C. Nordling, A. Wännström, J. Opt. Soc. Am. B **13**, 1650 (1996)
32. M. Gallardo, M. Raineri, M. Giuliani, C. Lagorio, S. Padilla, R. Sarmiento, J.G. Reyna Almandos, J. Quant. Spectrosc. Radiat. Transfer **95**, 365 (2005)
33. K.-T. Cheng, Y.-K. Kim, J. Opt. Soc. Am. **69**, 125 (1979)
34. L.J. Curtis, D.G. Ellis, I. Martinson, Phys. Rev. A **51**, 251 (1995)
35. C. Lavin, M.A. Almaraz, I. Martin, Z. Phys. D **34**, 143 (1995)
36. I. Martin, M.A. Almaraz, C. Lavin, Z. Phys. D **35**, 239 (1995)
37. H.-S. Chou, W.R. Johnson, Phys. Rev. A **56**, 2424 (1997)
38. J. Migdalek, M. Garmulewicz, J. Phys. B **33**, 1735 (2000)
39. U.I. Safronova, I.M. Savukov, M.S. Safronova, W.R. Johnson, Phys. Rev. A **68**, 062505 (2003)

40. S. Bashkin, R. Hallin, J. Leavitt, U. Litzén, D. Walker, Phys. Scr. **23**, 1981, 5
41. V. Kaufman, J. Sugar, Phys. Scr. **24**, 738 (1981)
42. V. Kaufman, J. Sugar, J. Opt. Soc. Am. B **1**, 38 (1984)
43. M. Gallardo, R. Sarmiento, M. Raineri, J. Reyna Almandos, Proc. SPIE **3572**, 547 (1999)
44. S.S. Churilov, Y.N. Joshi, Phys. Scr. **65**, 40 (2002)
45. G. O'Sullivan, J. Phys. B **15**, L765 (1982)
46. R.D. Cowan, *The Theory of Atomic Structure and Spectra* (Univ. of California Press, Berkeley, 1981)
47. P. Quinet, P. Palmeri, É. Biémont, M.M. McCurdy, G. Rieger, E.H. Pinnington, M.E. Wickliffe, J.E. Lawler, Mon. Not. R. Astron. Soc. **307**, 934 (1999)
48. J. Migdalek, W.E. Baylis, J. Phys. B **11**, L497 (1978)
49. S. Fraga, J. Karwowski, K.M.S. Saxena, *Handbook of Atomic Data* (Elsevier, Amsterdam, 1976)
50. P.H. Norrington; see the site `http://www.am.qub.ac.uk/DARC` (2002)
51. I.P. Grant, B.J. McKenzie, P.H. Norrington, D.F. Mayers, N.C. Pyper, Comput. Phys. Commun. **21**, 207 (1980)
52. B.J. McKenzie, I.P. Grant, P.H. Norrington, Comput. Phys. Commun. **21**, 233 (1980)
53. I.P. Grant, B.J. McKenzie, J. Phys. B **13**, 2671 (1980)
54. L.W. Fullerton, G.A. Rinker, Phys. Rev. A **13**, 1283 (1976)
55. P.J. Mohr, Ann. Phys. **88**, 52 (1974)
56. P.J. Mohr, Phys. Rev. Lett. **34**, 1050 (1975)
57. *Beam-foil spectroscopy*, edited by S. Bashkin (Springer-Verlag, Berlin, 1976)
58. X. Tordoir, H.P. Garnir, P.-D. Dumont, Nucl. Instrum. Methods B **140**, 251 (1998)
59. R. Hutton, Y. Zou, S. Huldt, I. Martinson, K. Ando, B. Nyström, T. Kambara, H. Oyama, Y. Awaya, Phys. Scr. **T80**, 552 (1999)
60. F.S. Garnir-Monjoie, Y. Baudinet-Robinet, H.P. Garnir, P.D. Dumont, J. Phys. **41**, 41 (1980)
61. L.J. Curtis, H.G. Berry, J. Bromander, Phys. Lett. A **34**, 169 (1971)
62. F. Acton, *Numerical methods that work* (Harper Row, 1970), p. 253